The Effect of Input Parameters on Visco-Elastic Models of Crustal Deformation.

F. Lorenzo-Martín[1], R. Wang[2] and F. Roth[2]

(1) Institute of Geology, Mineralogy and Geophysics, Ruhr University Bochum,
D-44780 Bochum, Germany
(2) GeoForschungsZentrum Potsdam (GFZ), Telegrafenberg,
D-14467 Potsdam, Germany

ABSTRACT

The increasing quality of data on time-dependent deformation of the Earth's surface can be used to extract more details on the spatial and temporal development of earthquake-related crustal deformation. Different variables are involved in these processes, some of them more accurately determined than others. We modelled surface deformation on a subduction zone, in a medium composed of an elastic layer over an inelastic half-space. We analyse the effect that three of the less accurately determined variables (viscosity of the half-space, thickness of the elastic layer and dip angle of the fault plane) have on the displacement field. We show that the variation of model parameters leads to a stable variability distribution in the deformation fields. We show which is the most appropriate data to be used to derive values for the studied parameters. The best data to derive the value of the viscosity is the post-seismic deformation over the area where the rupture takes place, although any area with large magnitude post-seismic displacements can provide profitable data. For the thickness of the elastic layer it is also advisable to use post-seismic data from the area above the fault plane, whereas the dip is better determined by means of co-seismic data.

1. INTRODUCTION

1.1 Motivation

   Geodetic data on time-dependent deformation of the Earth's surface can be used as a basis to derive rheological parameters of the crust and upper mantle by forward modelling. With the installation of the GPS system, especially with the recently started continuous measurements and, at the same time, since more Interferograms of Synthetic Aperture Radar (InSAR) data are generated, the sampling rate in monitoring recent crustal movements has drastically increased. This high data quality can be used to extract more details on the space-time development of tectonic processes, especially earthquake-related crustal deformations, and their basic rheological parameters. However, the variables that influence these processes are numerous and the way they affect the deformations is very different. Therefore, it is important to study the effect of the variation of the input parameters before trying to model any real data on crustal deformation.
   Seismology provides accurate values for the magnitude of an event and its seismic moment. Also, the average displacement over the fault plane can be accurately calculated from those values. The distribution of aftershocks immediately after the event leads to information about the depth at which the crust starts to behave visco-elastically rather than elastically. Also the location and orientation of the rupture plane, as well as its length and width, can be deduced from the aftershock distribution or from fault plane solutions. Nevertheless, the depth for the elastic to visco-elastic border and the size and geometry of the fault plane cannot be inferred with the same accuracy as magnitude, seismic moment or average displacement over the fault plane.
   Information on surface rupture and deformation at certain points on the surface can be available from geological and geodetic observations. This can lead to further information about the event that caused the deformation and the area where it took place. In addition, post-seismic geodetic measurements on time-dependent deformation can provide information about the viscosity of the lower crust and upper mantle, as well as about the rheological law that governs the relaxation process. Nevertheless, this process takes place very slowly, covering time intervals much longer than those for which accurate geodetic measurements have been carried so far. For this reason, in our analysis of the rheology, we confine ourselves to cases with Maxwell rheology with different values for the viscosity.

1.2 The modelling

There are two main modelling concerns. Firstly, the results should provide values that are in the range of what is measurable. Interpretations would be useless if the results from modelling are too small to exceed the resolution of real measurements. Secondly, it is important to check for the stability and uniqueness of the solution when we derive any source parameter from measured data. We must show that a best-fitting model can be found, so that we can find the most likely values for our parameter set. Also, we have to study which parameters influence the results, and how strong this influence is.

In our study, we fix the parameters that are usually accurately determined: seismic moment, average displacement over the fault plane and elastic rock properties for the layered half-space. The displacement on the fault plane is taken to be the same all over the rupture surface: there is no need to complicate the model excessively and, in addition, there is no evidence that it might be more realistic to split the whole rupture surface into patches with different average displacement. Also, the size of the fault plane is not changed, in order to avoid making our analysis too extensive. We chose to model deformations on a medium with an elastic layer over a visco-elastic half-space, since this is a reasonable simplification that nevertheless represents the properties of the crust and upper mantle appropriately. Such a medium has been widely used in former publications (e.g. Cohen 1980a, 1980b, 1994, Rundle 1982, Fernández *et al.* 1996, 1998, Yu et al. 1996, 1999), although the study of the effects of the input parameters on crustal deformation is in general not as systematic and includes not as many studied parameters as in the present paper.

Cohen (1980a) shows the effect that a change in the rheological model has on the modelled results for a strike-slip source, and Cohen 1980b extends the study to the effects of the depth of the source, its length and width, and the lithospheric thickness. Rundle (1982) analyses the result of considering a thrust fault in a viscoelastic-gravitational model. Calculations for fault planes that break the elastic layer fully or only partially are compared. Also deformation caused by faults of different size is analysed, as well as the differences arising from considering a viscoelastic-gravitational medium instead of a purely viscoelastic one. Ma *et al.* (1994) studied the effect of the rock parameters, the depth and width of the source and its dip angle for a fault in a three-layer medium. Cohen (1994) analyses the effect of the viscosity when modelling a dip-slip fault. Also, deformation due to a fault with constant dip is compared to that due to a fault with a variable one. Fernández *et al.* (1996, 1998) and Yu *et al.* (1996, 1999) analyse the effect of gravity on the

results for a dipping thrust fault and for a strike-slip fault respectively. They also included calculations for two different dip angles, as well as for fault planes that break the elastic layer fully or only partially. Roy *et al.* (2000a, b) consider two layers over the half-space, to analysed how the rheological stratification within the crust affects the formation and long-term evolution of fault systems.

In the following study, three parameters are systematically varied: the thickness of the elastic layer, the viscosity of the underlying half-space and the dip angle of the fault plane. Values for these parameters are, as stated before, not very well determined. We analyse the effect that small changes on these three parameters have on the resulting deformation. We created a so-called Reference Model (from now on RM), with average values for the parameters and vary these to compare the effect that this variation has on the deformation. The deformation caused by the RM played the role of synthetic geodetic data that we tried to model by means of different sets of parameters.

For the RM we chose the parameters to represent an earthquake on a subduction zone. To be exact, some of the values were taken from a concrete case, namely the 1960 Valdivia earthquake, since we expect to apply our modelling to geodetic data related to this event in the immediate future. This event was the largest recorded in the last century, with a moment magnitude of 9.5 (Kanamori 1977). GPS measurements in 1994 and 1996 in Chile and Argentina (Klotz *et al*. 2001) show that the deformation associated to the earthquake can still be observed. However, we did not want to confine the analysis to this event, so several parameters were substituted by more general ones.

2. THE METHOD

We created software based on the dislocation theory, to obtain time-dependent crustal deformation due to motion in faults in mixed elastic/inelastic media. In this software, the source causing the deformation can be chosen from a wide range of possibilities, covering all known earthquake mechanisms: double-couple with any given orientation, explosion, horizontal/vertical single force, etc. Any number of layers, with arbitrary and independent thickness, can be used. Every layer can have different Lamé's constant λ and shear modulus μ, independent from one another, as well as different rheologies (Maxwell or Standard Linear Solid). The output field can be displacement, stress or strain. All these possibilities give the software great flexibility.

The program is based on the wavenumber integration method. In this method, the Fourier-Hankel transform is applied to the equations of motion and the complete deformation field is decomposed into cylindrical surface harmonics with a continuous space-time spectrum. All the work is done in two major steps:

1) calculations of the temporal and spatial spectra that are solutions of the transformed equations of motion depending only upon the depth, and

2) integration over the wavenumber (Hankel transform) and frequency (Fourier transform).

Usually, the spectra solutions are calculated by the Thomson-Haskell propagator algorithm. However, numerical results of this algorithm are unstable. The cause is the known loss-of-precision problem that arises due to numerical operations between single vectors with the same propagation direction but quite different amplitudes (Wang *et al.*, 2003). In the present program, an improved propagator algorithm is used, in which the loss-of-precision problem is fully avoided by an orthonormalization method introduced by Wang (1999). The improved propagator algorithm is not only stable and efficient, but also retains the simple form of the original Haskell's propagator formulism, which simplifies the comprehension of the method and its implementation. For details about the algorithm see Wang (1999) and Wang and Kümpel (2002).

The inelastic Green's functions are calculated with the correspondence principle. Let us suppose that we know the elastic solution of a problem in which a displacement or a stress step is applied to a body. If the fields and moduli are replaced by their Fourier transform, then the Fourier transform of the solution of the corresponding visco-elastic problem is obtained. This implies that, in the frequency-domain, the convolution between the time dependency of the source mechanism and the time dependency due to the relaxation of the material parameters in the inelastic layers is a simple multiplication. The solution itself can then be written down as the inverse Fourier transform.

3. VARIABILITY ANALYSIS

3.1 The Reference Model

As was already mentioned, some values for the RM were taken from the 1960 Valdivia earthquake. A reference value of 41 km was used for the

thickness of the elastic layer, in accordance with receiver function images across the southern Andes (Kind *et al.* 2001). Since our model considers horizontal layers, lateral inhomogeneities from the crust, typical of subduction zones, cannot be taken into account.

The dip angle of the fault plane was 20° for the Valdivia earthquake, with a depth for the upper limit of the rupture plane of 6 km (Barrientos and Ward 1990). These values were adopted for the RM (see Fig. 1). Although the rake differed slightly from 90° for this event, we modelled a pure dip-slip event, in order not to take too many parameters into account. An arbitrary slip of 5 m and a surface of 80×40 km² was taken. The reader must bear in mind that the slip on the fault plane influences the final deformation in a linear way, so re-scaling the results would be straightforward. Similar media to the one described has been used by Thatcher *et al.* (1980, 1984), Rundle (1982) or Fernández *et al.* (1996).
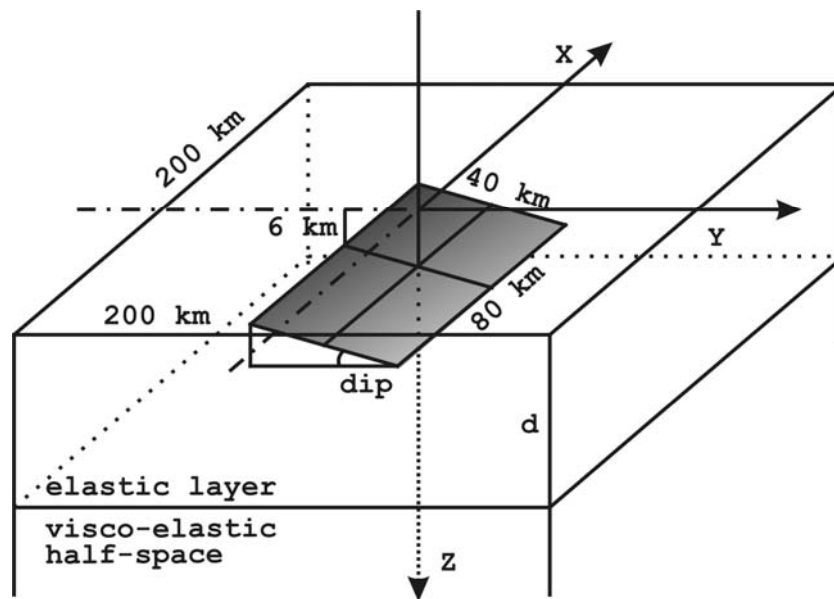

Figure 1: Schematic representation of the geometry of the fault and the medium used in the modelling. The half-space was made up of an elastic layer of variable thickness '**d**' and a visco-elastic half-space. The origin of the reference system is above the centre of the fault plane, with the x-axis parallel to the strike of the fault plane. The upper boundary of the fault plane is located at a depth of 6 km. The fault plane is 80 km long, 40 km wide and has a variable dip angle '**dip**'.

In addition to the geometry and position of the source, the physical media had to be described by means of some other values. We choose for these parameters representative values for a subduction zone (Dziewonski *et al.* 1981). The upper layer was given the following rock properties: Vp = 6.7 km/s; Vs = 3.87 km/s; $\rho = 2.9 \cdot 10^3$ kg/m^3.

The homogeneous half-space beneath this layer has Maxwell rheological properties. Piersanti (1999), compared post-seismic deformation data with synthetic results and concluded that the viscosity of the asthenosphere beneath the Chilean region should be between $8 \cdot 10^{19}$ and 10^{20} Pa·s. Vermeersen *et al.* (1998), by means of the study of the effects of the post-glacial rebound, obtained viscosities in the range of 10^{20} up to a few times 10^{20} Pa·s for the upper mantle. According to these studies, we decided to use a reference value of 10^{20} Pa·s for the viscosity.

The rock parameters for the half-space are: Vp = 8.0 km/s; Vs = 4.62 km/s; $\rho = 3.4 \cdot 10^3$ kg/m^3

The values listed above were used to create the RM. Subsequent models varying the dip angle, the thickness of the elastic layer and the viscosity of the inelastic half-space were also created. Then the deformation in these models was compared to the one from the RM.

3.2 The input parameters

Models with values for the viscosity from $0.5 \cdot 10^{20}$ Pa·s to $2.0 \cdot 10^{20}$ Pa·s in steps of a factor $\sqrt{2}$ were calculated. All the models had Maxwell rheological properties. The range covered by these values is almost one order of magnitude. The reason for this is that the viscosity is not very well known in most of the cases, and some studies show that traditional standard values used in simulations may be incorrect by up to one order of magnitude (Vermeersen *et al.* 1998).

For each of the values of the viscosity, the thickness of the elastic layer took also different values, from 35 km to 45 km every 2 km. This variation range reflects a realistic inaccuracy of 10% in the determination of this parameter.

For a subduction zone it would be realistic to increase the value of the dip angle with the depth. However, for simplicity, we decided to use a plane for the rupture area, and then vary the dip angle within values for this parameter at different depths in a subduction zone. For this reason, for every combination for the values of the former two parameters, values of the dip angle from 14° to 24° every 2° were also used. A total number of 180 different models were calculated.

Calculations were made for a grid of 41×41 test points, uniformly distributed every 5 km on a surface of 200×200 km² with the origin over the centre of the fault plane. However, in some cases only a trace of test points perpendicular to the strike of the fault plane is used to show the main dependencies.

3.3 Stability

To study the stability of the problem we compared the result of the RM with that of the other models. The difference in displacement was averaged for all the 1681 test points in the area above the rupture plane. The absolute deviation σ was calculated for every point as follows:

$$\sigma = |Ux_{RM} - Ux| + |Uy_{RM} - Uy|$$

where (Ux_{RM}, Uy_{RM}) are the displacement at that point in the x and y direction for the RM, and (Ux, Uy) are the same values for the compared model. Fig. 2 shows the averaged absolute deviations from the RM for the horizontal post-seismic displacement during the first 2 years after the event for different sets of parameters. In each of the panels there is only one local minimum: the deviations increase with the difference of the input parameters from the ones of the RM. Thus, our variations lead to a unique solution. It may be necessary though to have some limit for the variability of the parameters involved.

3.4 Effect of input parameters on co-seismic deformation

To avoid treating fault tip effects along strike we confine ourselves to a trace of 41 test points on the surface, perpendicular to the strike of the fault plane.
The upper panels on Figs. 3 and 4 show the co-seismic horizontal displacement (Uy, positive along dip direction) along the trace. Error bars are used to display the variability of the displacement with the dip angle of the fault plane (Fig. 3) or with the thickness of the elastic layer (Fig. 4). The fault plane dips towards positive values of the y-axis.
To analyse these curves in more detail, three test points were selected from this trace: B and C, 25 and 60 km distance from the centre of the fault, along dip, and A, 10 km distance in the opposite direction. The three points are marked with triangles on the upper panels of Figs. 3 and 4. Test point A is situated in the area where maximum co-seismic and post-seismic displacement occurs. Test point B is located on a plateau for the co-seismic
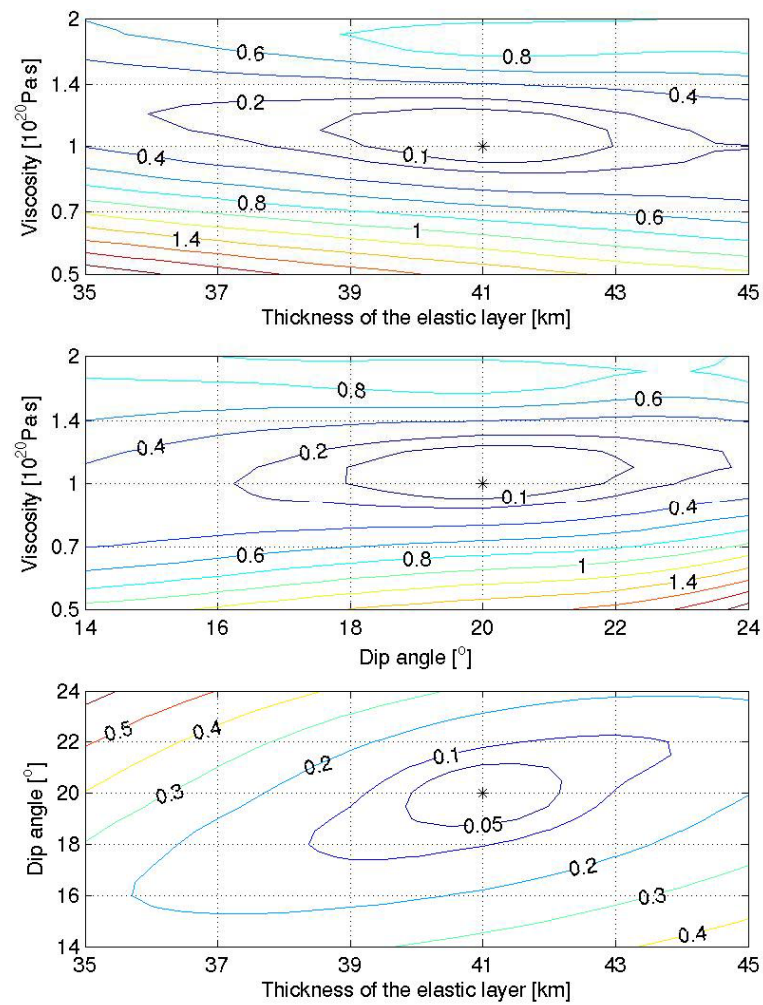
Figure 2: Averaged absolute deviations from the RM (mm) for the horizontal post-seismic displacement (first 2 years after the event) for different sets of parameters. The upper panel shows values for a fixed dip angle of 20°. For the middle panel a thickness of the elastic layer of 41 km was used. In the lower panel, a viscosity value of $1.0 \cdot 10^{20}$ Pa·s was used. The minimum (value 0, corresponding to the RM) is marked with a star on every panel. Values for the error increase as the compared models differ more from the RM.

displacement and, as will be seen later, in the area where the post-seismic deformation changes direction. It will also be shown later that test point C lies in the area where the post-seismic displacement reaches the greatest magnitude in the opposite direction to the overall displacement field. For these three points, the lower panels on Figs. 3 and 4 show the difference in displacement between the RM and models with other values for the parameters.

When the thickness of the elastic layer is fixed (Fig. 3), small variations in the dip angle correspond to noticeable changes of the deformation. This parameter influences the geometry and distribution of the deformation in such a strong way that deviations from the RM are very large. Basically, the difference in displacement increases as the magnitude of the displacement does, and deviations are remarkably large even for small magnitude displacements.

We conclude therefore that the effect of the dip angle in the co-seismic displacement is so strong that a value could be resolved best for this parameter by means of the analysis of data on the co-seismic displacements associated to a seismic event.

If the dip angle is fixed and the thickness of the elastic layer varied (Fig. 4, deviations have an exaggeration factor of 10 on the upper panel), the deviations for the co-seismic displacement are much smaller than in the previous case. There is also a rough direct relation between magnitude of the displacement and its variability. However, this does not hold true for the area where test point B is located. Deviations for this point may be too small to be measured (Fig. 4, lower panel). For the test points A and C, any change away from the RM leads to variations over 2 mm.

As we have just seen, the position of the test point can diminish the variability of the displacement drastically. In the case that measurements are taken at such points, it may not be possible to infer a value for the thickness of the elastic layer only by means of the analysis of the co-seismic deformation. Other information, like the fault plane solution or the distribution of aftershocks, may be needed to constrain the value of this parameter.

The reader should bear in mind that the difference in deformation associated to a change of the thickness of the elastic layer depends on the contrast in the two Lamé's constants between the elastic layer and the ones for the visco-elastic half-space. However, this study did not analyse this possibility of modifying the model, and was limited to the contrast induced by the relaxation with time of the physical rock parameters in the visco-elastic half-space.
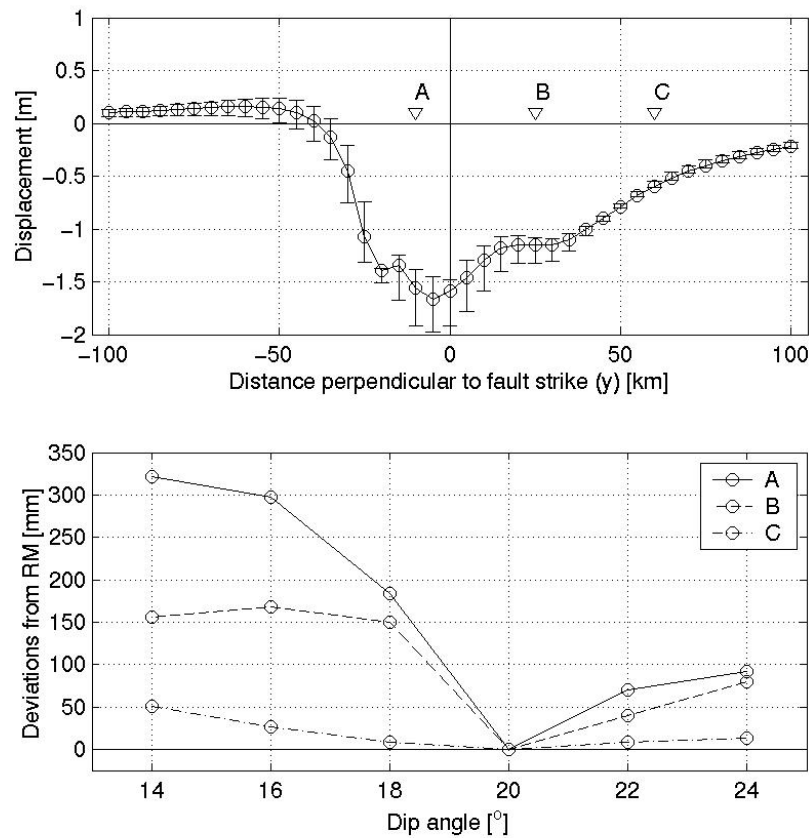
Figure 3: Co-seismic horizontal displacement (Uy) for a trace of points perpendicular to the strike of the fault plane. The fault plane dips towards positive values of the y-axis. The thickness of the elastic layer was fixed to 41 km. The upper panel shows the displacement together with its variability (as error bars) when different values for the dip angle of the fault plane are used (no vertical exaggeration for the deviations). The lower panel shows the deviations from the RM for the three points at the surface: A (y = -10 km), B (y = 25 km) and C (y = 60 km) for the different values of the dip angle of the fault plane. Even a small variation of the dip angle leads to notable changes in the displacement.
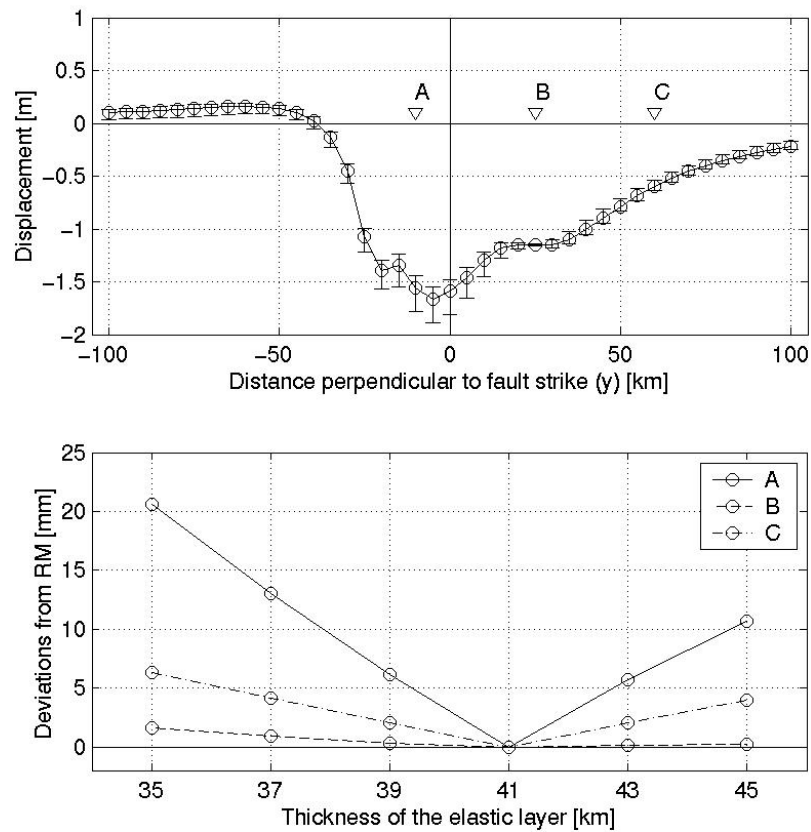
Figure 4: Co-seismic horizontal displacement (Uy) for a trace of points perpendicular to the strike of the fault plane. The fault plane dips towards positive values of the y-axis. The dip angle was fixed to 20°. The upper panel shows the displacement together with its variability (as error bars) when different values for the thickness of the elastic layer are used (vertical exaggeration for the deviations: factor 10). The lower panel shows the deviations from the RM for the three points at the surface: A (y = -10 km), B (y = 25 km) and C (y = 60 km) for the different values of the thickness of the elastic layer. In this case, deviations for point B are very small.

3.5 Effect of input parameters on post-seismic deformation

We consider again the trace of 41 test points perpendicular to the strike of the fault plane. For these points, the circles in Fig. 5 show the horizontal post-seismic displacement in the y-direction for the first two years after the event. Its variation with the three studied parameters is represented by means of error bars. The fault plane dips towards positive values of the y-axis.

Varying the three parameters at the same time leads to big changes in the results. We only include the results starting from the value $\eta = 0.7 \cdot 10^{20}$ Pa·s. A value for the viscosity of $0.5 \cdot 10^{20}$ Pa·s only leads to bigger deviations. The values for the parameters that lead to the top and bottom values for the displacement are listed in Table 1.

Although the variability of the displacement is remarkable, it is not evident which variables have a stronger influence, and how this influence depends on the distance to the fault plane. This is now analysed in greater detail, first taking account of the location of the test point, and then varying only one of the parameters at a time.

3.5.1 Distance to the fault plane

If we consider the test points A, B and C as before, we again observe that the different parameters have a different influence on the deformation depending on the location. Figure 6 shows the deviations for the post-seismic displacement for the first two years after the event at these three test points. At test point A (first column in Fig. 6), located in the area of maximum deformation, deviations are on average greater than at the other two test points. In the two lower panels, variations with the dip angle are much smaller than those with the other two parameters, showing that varying the dip angle does not influence the results as much as the viscosity or the thickness of the elastic layer. The same holds true for test point C (last column in Fig. 6), although in this case the magnitude of the deviations is much smaller.

On the contrary, test point B (middle column in Fig. 6) shows that deformation in this area is actually more sensitive to the dip angle than to the other two parameters (lower two panels, middle column in Fig. 6). However, the magnitude of these deviations is still smaller than the deviations at test point A.

It should be noticed that each panel in this figure shows results for a single test point. In some cases there are other local minima apart from the one corresponding to the RM, or the models around the latest show small devia-
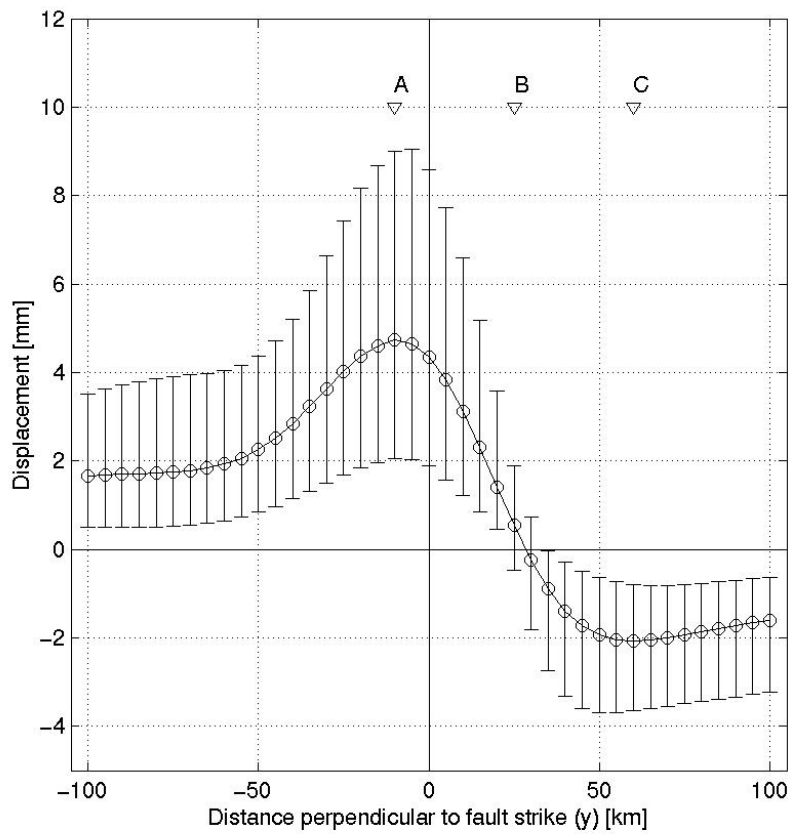
Figure 5: Horizontal post-seismic (first two years after the event) displacement perpendicular to the strike of the fault plane for a trace of points perpendicular to the strike of the fault plane. For every point, the displacement corresponding to the RM is plotted (circles), together with its variation when the thickness of the elastic layer, the viscosity of the half-space and the dip angle of the fault plane changes. See Table 1 for the parameters that lead to the maximum or minimum displacement.

Table 1: Value list for the model parameters that lead to the top or bottom values for horizontal displacements when the three parameters change. For example, on the surface, 5 km away from the origin of coordinate in the dipping direction, the model that leads to the maximum displacement is the one with a dip angle of 16°, an elastic layer 35 km thick and a viscosity of $0.7 \cdot 10^{20}$ Pa·s. The values for the resulting displacement were used for the error bars on Fig. 5.

Distance to fault plane centre [km]	Model parameters leading to error bars					
	Top			Bottom		
	Dip angle [°]	Thickness [km]	Viscosity $[10^{20}\text{Pa·s}]$	Dip angle [°]	Thickness [km]	Viscosity $[10^{20}\text{Pa·s}]$
-100 to -15	24	35	0.7	14	45	2.0
-10	18	35	0.7	14	45	2.0
-5	18	35	0.7	24	45	2.0
0	18	35	0.7	22	45	2.0
5	16	35	0.7	24	45	2.0
10	14	35	0.7	24	45	2.0
15	14	35	0.7	24	45	2.0
20	14	35	0.7	24	45	2.0
25	14	35	0.7	24	35	0.7
30	14	45	0.7	24	35	0.7
35 to 100	14	45	2.0	24	35	0.7

tion. This simply demonstrates that it would be very difficult to infer the value of our parameters from the deformation observed at a single test point.

These results provide important information on the optimal location of the test points required to extract information from post-seismic data. Measurements around test point A or C will be useful for determining the thickness of the elastic layer or the viscosity of the half-space, but will provide poor information on the dip angle, whereas the area around point B will behave the opposite way.

The area of maximum deformation provides data that can be measured easily. In addition, the results depend heavily on the viscosity, so interpretation of the measurements could provide reliable values for this para meter. Measurements around test points B and C, although smaller in magnitude, could be useful for obtaining results about the other two variables if, as might be the case, no reliable value is available for the viscosity.
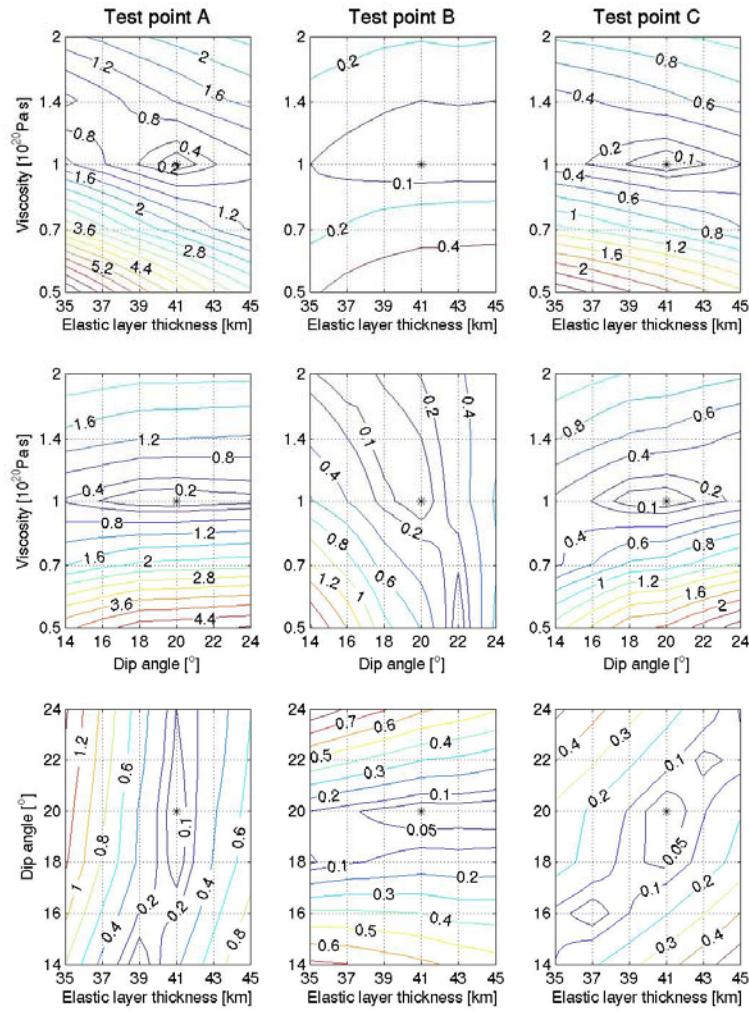
Figure 6: deviations from the RM (mm) for the post-seismic displacement for the first two years after the event for points A, B and C, as indicated in Fig. 5. The first row shows values for a fixed dip angle of 20°. For the second row a thickness of the elastic layer of 41 km was used. In the third row, a viscosity value of $1.0 \cdot 10^{20}$ Pa·s was used. The minimum, corresponding to the RM, is marked with a star on every panel.

3.5.2 Effect of single input parameters

We plotted the horizontal (Uy) post-seismic displacement for the trace of test points perpendicular to the fault plane strike (Fig. 7). On the upper panel, we represent the variability of the displacement with the viscosity of the half-space. Once again, we only include the results starting from the value $\eta = 0.7 \cdot 10^{20}$ Pa·s, since a value for the viscosity of $\eta = 0.5 \cdot 10^{20}$ Pa·s only leads to bigger deviations from the RM.

The magnitude of the displacement increases as the viscosity decreases and vice versa. The values for the viscosity that lead to the greater or smaller displacement are listed in Table 2. At test points where the displacement is large, there is also large variability of the results. This indicates that data from areas of large deformation is appropriate for finding a value for the viscosity.

The central panel of Fig. 7 shows the same curve with its variability when only the thickness of the elastic layer changes. Basically, once again there is an inverse relationship between this parameter and the magnitude of the displacement: smaller magnitude displacements correspond to the model with a thicker elastic layer. Nevertheless, 25 km away from the centre, where the displacement almost vanishes, the maximum displacement corresponded to the RM itself (see triangles in Fig. 7, central panel). The values from the rest of the models are smaller. The model that leads to the minimum displacement at this test point is the one with an elastic layer 35 km thick, the same as for all the test points with negative displacement (see Table 2). In this case, the greatest variation occurs where the deformation is greater as long as the displacements are positive (along dip). When the displacement takes negative values, this relation does not hold, and the magnitude of the deviations from the RM is generally smaller. This means that data from the area of maximum displacements is the most appropriate when looking for a value for the elastic layer thickness.

The variation of the dip angle of the fault plane affects the displacement in a more complicated way (lower panel of Fig. 7). The dip angle values that provide the top and bottom values for the displacements change more smoothly than in the case of the other two parameters (see box 'a' in Fig. 7 and Table 2). Moreover, box 'b' shows an area where changing the parameters for the model can lead to a change in the direction of the displacement. In addition, the greatest variability of the displacement does not correspond to the test points where the magnitude of the displacement is greatest (although this was the case for the co-seismic displacement, Fig. 2). The dip angle, in contrast to the viscosity or the thickness of the elastic layer,
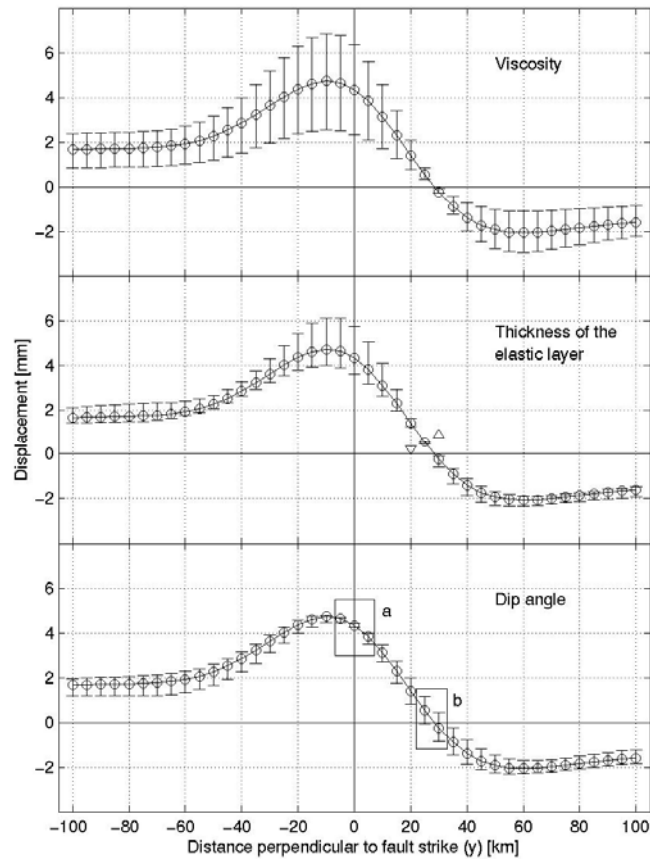
Figure 7: Horizontal post-seismic (first two years after the event) displacement Uy for a trace of points perpendicular to the strike of the fault plane. In every panel the displacement is plotted with circles, and for every point also the variation of the displacement with one parameter is included. The upper panel shows the variation when viscosity changes, whereas the middle and lower panels show the variation with the thickness of the elastic layer and the dip angle of the fault plane, respectively. The triangles in the middle panel show the test point where the thickness of the elastic layer for maximum and minimum displacement changes. Box 'a' in the lower panel shows the area for which the dip angle of the fault plane for maximum and minimum displacement changes. Box 'b' shows the area for which a change in the dip angle can lead to a change in the sign of the displacement. For the parameters that lead to the maximum or minimum displacement see Table 2.

Table 2: Value list for the model parameters that lead to the top or bottom values for horizontal displacements when one of the parameters changes. For example, on the surface, 5 km along dip from the origin of the coordinate system, when only the viscosity changes, the model that leads to the maximum displacement is the one with a viscosity of $0.7 \cdot 10^{20}$ Pa·s. The values for the resulting displacement were used for the error bars on the upper panel (half-space viscosity), central panel (thickness of the elastic layer) and lower panel (dip angle) on Fig. 7.

Distance to fault plane centre [km]	Model parameters leading to error bars					
	Half-space viscosity [10^{20}Pa·s]		Thickness of the elastic layer [km]		Dip angle of fault plane [°]	
	Top	Bottom	Top	Bottom	Top	Bottom
-100 to -10	0.7	2.0	35	45	24	14
-5	0.7	2.0	35	45	18	14
0	0.7	2.0	35	45	18	22
5	0.7	2.0	35	45	16	24
10	0.7	2.0	35	45	14	24
15	0.7	2.0	35	45	14	24
20	0.7	2.0	35	45	14	24
25	0.7	2.0	41	35	14	24
30 to 100	2.0	0.7	45	35	14	24

is a geometrical variable that only affects the distribution of the displacements and not their development in time. These facts stress the importance of observation points in the area where the post-seismic displacement changes direction. Data from this area should be used to resolve the value of the dip angle.

4. CONCLUSIONS

Earthquake-related crustal deformation processes involve multiple variables, some of which are less precisely determined than others. Former works on forward modelling usually include no analysis of the effect of these variables on the deformation or this analysis is not systematic (Cohen 1980, Thatcher *et al.* 1979). Furthermore, not always more than one variable is analysed , and when several are, the study is constrained to not more than two or three values for each variables (Fernández *et al.* 1996, Yu *et al.* 1996). In

the present study, the effect of three different variables is analysed in detail to ascertain how heavily results depend on which parameter. From this analysis the following conclusions were derived:

1- When analysing the co-seismic displacement, a strong dependency on the dip angle of the fault plane is found. Points with large displacements show also a large variability when the dip angle varies. The area over the rupture plane is the one where the largest displacements take place. Therefore, surface measurements in this area are the most suitable for ascertaining the most likely value for the dip angle.

By contrast, varying the thickness of the elastic layer leads to small differences, which are especially small in the area where the post-seismic deformation changes direction. This indicates that co-seismic displacement measurements, especially around the mentioned area, are not recommendable for trying to ascertain an accurate value for this parameter.

2- In the analysis of the post-seismic deformation we find that, on average, deviations from the RM are of a greater magnitude over the rupture plane than further towards the dipping direction. In this area, the dip angle does not influence the results as much as the other two parameters. Further along the dipping direction, in the area where post-seismic displacement changes sign, this reverses, and the dip angle becomes the most influential parameter. Further on, where the displacement reaches its highest point in the direction towards negative y-values, once more the dip angle has less of an effect than the other two parameters.

Accordingly, measurements in areas of large post-seismic displacements are suitable for deriving a value for the viscosity. In particular, above the rupture area, values depend heavily on this parameter. The same area can also provide data that is useful for ascertaining the thickness of the elastic layer, although for this parameter the area where the minimum displacement occurs is not as appropriate as for the viscosity.

The dip angle, in general, cannot be accurately derived using post-seismic deformation data. The magnitude of the variability associated with this parameter is very small. The best place to find a value for this parameter is the area where the post-seismic displacement changes direction.

ACKNOWLEDGMENTS

REFERENCES

BARRIENTOS, S. E., AND WARD, S. N. (1990): «The 1960 Chile earthquake: inversion for slip distribution from surface deformation», *Geophys. J. Int.,* **103**, 589-598.

COHEN, S. C. (1980): «Postseismic viscoelastic surface deformation and stress 1. Theoretical considerations, displacement, and strain calculations», *J. Geophys. Res.*, **85**, 3131-3150.

COHEN, S. C. (1980): «Postseismic viscoelastic surface deformation and stress 2. Stress theory and computation; Dependence of displacement, strain, and stress on fault parameter», *J. Geophys. Res.*, **85**, 3151-3158.

COHEN, S. C. (1994): «Evaluation of the importance of model features for cyclic deformation due to dip-slip faulting», *Geophys. J. Int.*, **119**, 831-841,

DZIEWONSKI, A. M. AND ANDERSON, D. L. (1981): «Preliminary reference Earth model», *Phys. Earth Planet. Inter.*, **25**, 297-356.

FERNÁNDEZ, J., YU, T. T. AND RUNDLE, J. B. (1996): «Horizontal viscoelastic-gravitational displacement due to a rectangular dipping thrust fault in a layered Earth model», *J. Geophys. Res.*, **101**, 13581-13594.

FERNÁNDEZ, J., YU, T. T. AND RUNDLE, J. B. (1998): «Correction to "Horizontal viscoelastic-gravitational displacement due to a rectangular dipping thrust fault in a layered Earth model" by José Fernández, Ting-To Yu and John B. Rundle», *J. Geophys. Res.*, **103**, 30283-30286.

KANAMORI, H. (1977): «Energy release in great earthquakes», *J. Geophys. Res.*, **82**, 2981-2987.

KIND, R., BOCK G. AND YUAN, X. (2001): *The Structure of the Lower Plate from Broad-band Seismology*, report for the research period 1999-2001, SFB 267 (Collaborative Research Center 'Deformation processes in the Andes – Interaction between endogenic and exogenic processes during subduction orogenesis').

KLOTZ, J., KHAZARADZE, G., ANGERMANN, D., REIGBER, C., PERDOMO, R. AND CIFUENTES, O. (2001): «Earthquake cycle dominates contemporary crustal deformation in Central and Southern Andes», *Earth and Planetary Science Letters,* **193** (3-4), 437-446.

MA, X. Q. AND KUSZNIR, N. J. (1994): «Effects of rigidity layering, gravity and stress relaxation on 3-D subsurface fault displacement fields», *Geophys. J. Int.,* **118**, 201-220,

PIERSANTI, A., (1999): «Postseismic deformation in Chile: Constraints on the asthenospheric viscosity», *Geophys. Res. Letters,* **26**, 3157-3160,

ROY, M. AND ROYDEN, L. H. (2000): «Crustal rheology and faulting at strike-slip plate boundaries 1. An analytical model», *J. Geophys. Res.*, **105**, 5583-5597.

ROY, M., AND ROYDEN, L. H., (2000): «Crustal rheology and faulting at strike-slip plate boundaries 1. Effects of lower crustal flow», *J. Geophys. Res.*, **105**, 5599-5613

RUNDLE, J. B., (1982): «Viscoelastic-gravitational deformation by a rectangular thrust fault in a layered Earth», *J. Geophys. Res.*, **87**, 7787-7796.

THATCHER, W. AND RUNDLE, J. B. (1979): «A model for earthquake cycle in underthrust zones», *J. Geophys. Res.*, **84**, 5540-5556.

THATCHER, W., MATSUDA, T., KATO, T. AND RUNDLE, J. B. (1980): «Lithospheric loading by the 1896 Riku-u earthquake, Northern Japan: Implications for plate Flexure and Asthenospheric Rheology», *J. Geophys. Res.*, **85**, 6429-6435.

THATCHER, W. AND RUNDLE, J. B. (1984): «Viscoelastic coupling model for the cyclic deformation due to periodically repeated earthquakes at subduction zones», *J. Geophys. Res.*, **89**, 7631-7640.

VERMEERSEN, L. L. A., SABADINI, R., DEVOTI, R., LUCERI, V., RUTIGLIANO, P., SCIARRETTA, AND BIANCO, G. (1998): «Mantle viscosity inferences from joint

inversion of pleistocene deglaciation-induced changes in geopotential with a new SLR analysis on a polar wander», *Geophys. Res. Letters,* **25**, 4261-4264.

WANG, R., (1999): «A simple orthonormalization method for the stable and efficient computation of Green's functions», *Bull. Seism. Soc. Am.,* **89**, 733-741.

WANG, R. AND KÜMPEL, H.-J. (2002): «Poroelasticity: efficient modelling of strongly coupled, slow deformation processes in multi-layered half-space», *Geophysics*, published electronically September 23.

WANG, R., LORENZO, F. AND ROTH, F. (2003): «Computation of deformation induced by earthquakes in a multi-layered elastic crust – FORTRAN programs EDGRN/EDCMP», *Computers & Geosciences,* **29**/2, 195-207.

YU, T. T., RUNDLE, J. B. AND FERNÁNDEZ, J. (1996): «Surface deformation due to a strike-slip fault in an inelastic gravitational layer overlaying a viscoelastic gravitational half-space», *J. Geophys. Res.*, **101**, 3199-3214.

YU, T. T., RUNDLE, J. B. AND FERNÁNDEZ, J. (1999): «Correction to "Surface deformation due to a strike-slip fault in an inelastic gravitational layer overlaying a viscoelastic gravitational half-space" by Ting-To Yu, John B Rundle and José Fernández», *J. Geophys. Res.*, **104**, 15313-15315.